New Developments in Elucidation of Hydrogen Embrittlement Phenomena from the Incubation Stage to Fracture

ISIJ International, Vol. 64 (2024), No. 4, pp. 756–764
https://doi.org/10.2355/isijinternational.ISIJINT-2022-356

Influence of High Concentration Vacancy-Type Defects on the Mobility of Edge Dislocation in α-Iron: An Atomistic Investigation

Sunday Temitope OYINBO[1)]* and Ryosuke MATSUMOTO[2)]

1) Nagamori Institute of Actuators, Faculty of Engineering, Kyoto University of Advanced Science, 18, Yamanouchi-Gotandacho, Ukyo-word, Kyoto, 615-8577 Japan.
2) Department of Mechanical and Electrical Systems Engineering, Faculty of Engineering, Kyoto University of Advanced Science, 18, Yamanouchi-Gotandacho, Ukyo-word, Kyoto, 615-8577 Japan.

(*Received August 10, 2022; Accepted December 20, 2022; Advance online published December 29, 2022; Published February 28, 2024*)

Many vacancy-type defects (vacancy, vacancy clusters, and hydrogen-vacancy complexes) are generated in metals by plastic deformation in hydrogen environments. In this study, we use extensive molecular dynamics calculations based on a highly accurate interatomic potential to examine how vacancy-type defects affect the mobilities of edge dislocations in α-iron at a temperature range of 300–500 K and a dislocation speed V_d range of 0.1–10 m/s. Under all conditions, the edge dislocation absorbs the vacancies along the slip plane and causes them to migrate with the edge dislocation. Although the necessary shear stress to glide edge dislocation in α-iron containing vacancy increases with dislocation speed, the effect is small compared to the hydrogen effects. The dislocation absorbs the hydrogen-vacancy complex along the slip plane and causes the hydrogen and the jog to migrate with the edge dislocation at low dislocation velocity regimes ($V_d \leq 0.1$ m/s). Therefore, the hydrogen-vacancy complex exerts a continuous drag effect on the dislocation. At higher dislocation speeds ($V_d \geq 1$ m/s), hydrogen does not migrate with the dislocation, resulting in the formation of isolated hydrogen detached from the dislocation and diffused into the material; only vacancy is absorbed. When multiple hydrogen-vacancy complexes are arranged along the slip plane, the dislocation absorbs them if they interact with dislocation at different points rather than at a single point to avoid the formation of a large jog at the colliding segment, and the required shear stress increases as the hydrogen atoms in the dislocation core increase.

KEY WORDS: edge dislocation; molecular dynamics; iron; hydrogen; vacancy; shear stress.

1. Introduction

The mechanical properties of various metallic materials are degraded by hydrogen. The challenge must be addressed head-on if society is to embrace a hydrogen economy in the future. Many models of hydrogen embrittlement have been proposed, such as the increase in localized plasticity, loss of cohesive strength, vacancy damage accumulation, fracture surface emission of dislocations, and more.[1)] The interaction of hydrogen with lattice defects is the basis of macroscopic changes in mechanical properties, such as yielding stress, hardening behavior, and embrittlement.[2–4)] Although intensive studies have been continued, the detailed process leading to the degradation of mechanical properties by hydrogen remains unknown, even for a simple material such as α-iron.

High concentration vacancy exists in various metals after plastic deformation in the presence of hydrogen, and there is a relationship between their existence and the metals' mechanical properties.[5–9)] Some thermal annealing recovers ductility by annihilating or changing the existing state of those defects. The amount of hydrogen that can be dissolved in metal is too small to experimentally measure the distribution.[10)] Understanding microscopic mechanisms, such as dislocation migration and interactions in the presence of hydrogen and vacancy can be accomplished through modeling and numerical simulation.[11–14)] Regarding the hydrogen effect on vacancies, numerical studies on α-iron have shown that vacancies and hydrogen have a large energetic driving force that can be exploited.[4,7,8,15–17)] Many first-principle computations have demonstrated that multiple hydrogen atoms can be trapped within monovacancy (V1) in α-iron as V1 + nH = V1Hn,[18–21)] and the product (V1Hn) is a hydrogen-vacancy complex with a high degree of stability. One V1 can trap up to six hydrogen atoms, while V1H2 is the most stable complex at room temperature in a moderate hydrogen environment.[18,22)] V1Hn complexes can also be

* Corresponding author: E-mail: sunday.t.oyinbo@kuas.ac.jp

found in various body center cubic (bcc) and face-centered cubic (fcc) metals.[19,23] Hydrogen significantly reduces vacancy diffusion and suppresses its annihilation through diffusion. Therefore, the vacancy concentration increases abnormally as plastic deformation progresses.[22]

Hydrogen-vacancy complexes interact with dislocations during mechanical deformation.[8] Therefore, understanding how their interactions affect dislocation mobility is critical. However, little is known about its influence on dislocation mobility at different temperatures at extremely high concentrations, which can be realized in a hydrogen environment. Therefore, the effect of such vacancy-type defects is a pertinent topic that demands additional inquiry and investigation. This examines how vacancy-type defects influence edge dislocation mobility and migration behavior in α-iron at different velocities and temperatures using comprehensive molecular dynamics (MD) computations based on a highly accurate interatomic potential. Although the main target in this study is the interaction of dislocations with vacancy-type defects, the interaction with hydrogen atoms is included for comparison because the interatomic potential used in this study differs from that in a previous study.[24] The previous study contained a detailed MD analysis of the interaction between an edge dislocation and hydrogen.[25–27]

2. Methodology

2.1. Molecular Dynamics Method

Large-scale Atomic/Molecular Massively Parallel Simulator (LAMMPS)[28] was used to execute the molecular dynamic simulations, while an open visualization tool (OVITO)[29] was used to visualize the atomic configurations. The α-iron single crystal contains 6 210 atoms (**Fig. 1**), with dimensions of ~8.5 nm in x, 4.0 nm in y, and 2.0 nm in z. The calculation cell was set up (Fig. 1) along [111], [$\bar{1}\,\bar{1}$2], and [1$\bar{1}$0] orientations for x, y, and z directions, respectively. Periodic boundary conditions (PBC) were enforced in both the x and z axes. A nonperiodic boundary condition was imposed in the y-direction by introducing a vacuum layer. The dislocation along [1$\bar{1}$0] on ($\bar{1}\,\bar{1}$2) with Burgers vector 1/2[111] was introduced in the simulation model, as in previous studies of dislocation motion.[26] Then, using the procedure shown in the following paragraph, vacancy and hydrogen were introduced. The upper and lower three atomic layers were fixed in the x- and y-direction, and relaxation were carefully performed for 50 ps at an intended constant temperature. A constant x-velocity was applied to the atoms in the upper and lower regions in different directions to perform boundary velocity-controlled loading. The boundary atom velocity is defined to enforce the intended dislocation velocity. MD Simulations were performed using Berendsen thermostat[30] to regulate the temperature in all cases. The simulation runs with a time step of 0.1 fs throughout. The edge dislocations were investigated using the dislocation extraction method (DXA)[31] and common neighbor analysis (CNA).[32] The calculation conditions are summarized in **Table 1**.

In this study, five simulation cells were created and used for dislocation mobility simulations, allowing us to investigate the effect of hydrogen, vacancies, and hydrogen-vacancy complex on dislocation mobility (**Table 2**). Trial 1 is single-crystal α-iron devoid of hydrogen and vacancy. Trial 2 corresponds to n-hydrogen atoms discretely distributed along the dislocation core in the initial state. In this scenario, one, two, five, and ten hydrogen atoms were distributed into the dislocation core. The hydrogen concentration for one, two, five, and ten hydrogen atoms corresponds to 0.5, 1, 2.5, and 5 nm^{-1} along the dislocation line. The corresponding hydrogen gas pressure, which realizes these hydrogen concentrations at thermal equilibrium at room temperature, is lower than atmospheric pressure, even for the highest hydrogen concentration.[27] In Trial 3, the simulation cell contained one monovacancy (1V1), two monovacancies (2V1), or one divacancy (1V2) along the dislocation

Table 1. Calculation conditions for MD simulations.

	Details
Model size [nm^3]	8.5 × 4.0 × 2.0
Duration of simulation [ns]	0.1–100
Timestep [fs]	0.1
Dislocation velocity [m/s]	0.1, 1, and 10
Interatomic potential	Embedded-atom-method (EAM)[37]
Temperature [K]	Constant at 300, 350, 400, 450, and 500

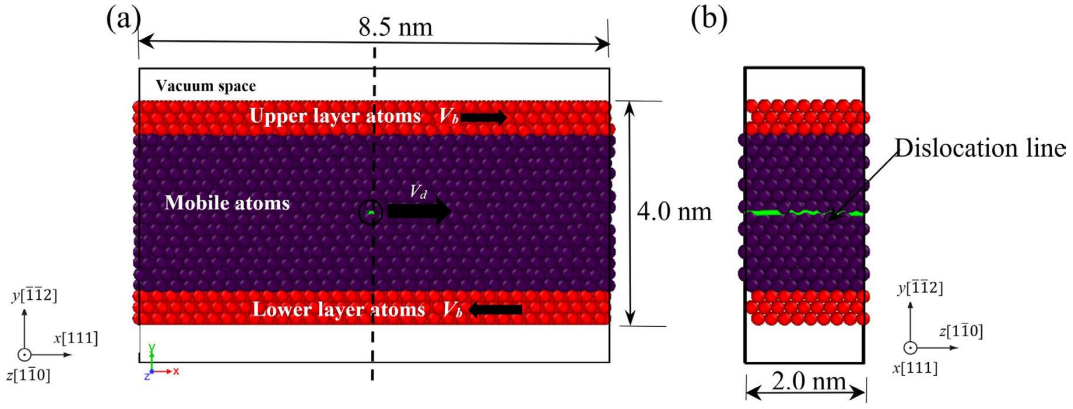

Fig. 1. Geometry and boundary conditions of the simulation model: (a) Front (z-axis) view showing the upper and lower boundary atoms (red atoms), the direction of edge dislocation velocity (V_d), boundary atoms velocity (V_b), and mobile atoms (purple atoms) (b) Cross-sectional (x-axis) view showing dislocation segment in the green line. (Online version in color.)

path (**Fig. 2**). The vacancy concentration in this analysis is 0.016% or 0.032%, which is lower than the predicted order of achievable vacancy concentration during plastic deformation in a hydrogen environment.[8] Trial 4 involves a hydrogen-vacancy complex. One, two, and three hydrogen atoms are seperately added into the formed vacancy to generate the hydrogen-vacancy complex. Trial 5 contains two simulation models with five VH2 complexes along the slip plane of different configurations. The first model contained five VH2 complexes in a line along the dislocation path. The second model also contains five VH2 complexes, which are distributed at different positions in the z-coordinate on the dislocation path.

The temperature used in this study ranges from 300 to 500 K to better understand how temperature affects edge dislocation mobility. Higher temperatures beyond room temperature are used to increase hydrogen mobility. The results for higher temperatures (≥ 500 K) are omitted for

Table 2. Summary of simulation models.

Trial	
1	Without hydrogen and vacancy (6 210 Fe atoms)
2	With One, two, five, and ten hydrogen atoms scattered discretely along the dislocation line (6 210 Fe atoms and 1–10 H atoms)
3	With one monovacancy (1V1), two monovacancies (2V1), and one divacancy (1V2) (6 208–6 209 Fe atoms)
4	With hydrogen-vacancy complex containing one to three hydrogen atoms (VH1, VH2, and VH3) (6 209 Fe atoms and 1–3 H atoms)
5	With five hydrogen-vacancy complexes (VH2) arranged on the slip plane (6 205 Fe atoms and 10 H atoms)

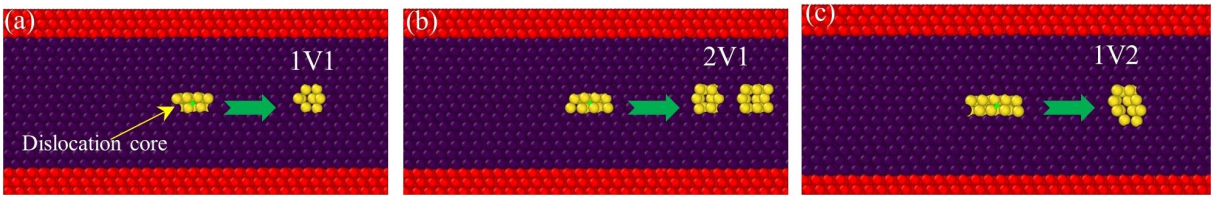

Fig. 2. The initial distribution of (a) 1V1 (b) 2V1, and (c) 1V2: The purple and yellow atoms represent Fe atoms with bcc structure and non-bcc structure (defects), respectively. The green arrow indicates the direction of edge-dislocation motion. (Online version in color.)

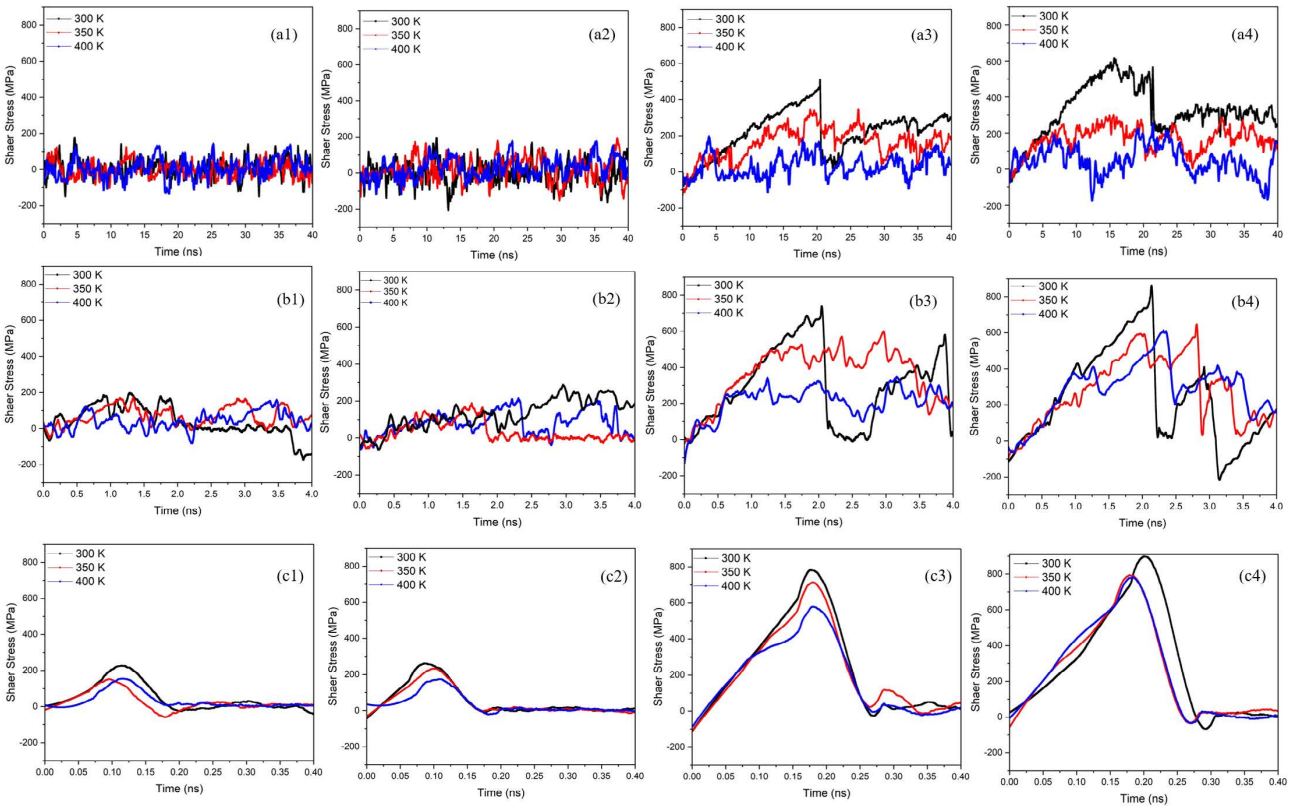

Fig. 3. Shear stress evolution with time at different temperatures for Trial 2 with one (C_H=0.5 nm^{-1})(a1, b1, and c1), two (C_H=1 nm^{-1})(a2, b2, and c2), five (C_H=2.5 nm^{-1})(a3, b3, and c3), and ten (C_H=5 nm^{-1})(a4, b4, and c4) hydrogen atoms: The dislocation velocity of (a1–a4), (b1–b4), and (c1–c4) are 0.1, 1, and 10 m/s, respectively. (Online version in color.)

the system with hydrogen because hydrogen atoms can easily escape from the dislocation at temperatures higher than 500 K.

2.2. Interatomic Potential Functions

Embedded-atom method (EAM) potentials were used to take into account the multiple-body effects associated with metallic bonding. These potentials have extensive use and success in the modeling of metallic materials.[33–36] The EAM potential created by M. Wen[37] for the Fe–H system was used to depict the force field in this study. This EAM potential was built using a comprehensive library of atom configurations and energies obtained from density functional theory (DFT) simulations, and it accurately recorded the hydrogen and iron interaction. This force field is accurate and dependable for modeling hydrogen interactions in α-iron, such as hydrogen bonding to open surfaces, dislocations, and vacancies, and it is useful for predicting hydrogen dissolution and diffusion.[37]

In metals and alloys, hydrogen-hydrogen interaction is critical in the hydrogen accumulation at defects, such as microvoids, grain boundaries, dislocations, vacancies, and surfaces, among other things. Previous studies have demonstrated that hydrogen-hydrogen interaction with hydrogen in T-sites is critical in the induction of false hydrogen aggregation in bcc Fe.[38] According to a recent study, the hydrogen-hydrogen bond with the hydrogen in O-sites is significantly more favorable than the interaction with hydrogen in T-sites, which is the primary cause of hydrogen aggregation.[39] Therefore, the EAM potential for the Fe–H system[37] contains appropriate DFT findings of the interactions of hydrogen-hydrogen with hydrogen in T-sites and O-sites[39] in their fitting targets for this potential to adequately characterize the hydrogen interaction in the bcc Fe lattice.

3. Results and Discussions

3.1. Influence of Vacancy on Edge Dislocation Motion

Figures 3 and **4** show the time evolution of shear stresses for Trials 2 and 3, respectively. The time average shear stresses calculated using the value after the dislocation collides with a hydrogen atom, a vacancy, or a vacancy-hydrogen complex are shown in **Table 3**. The average shear stress obtained from Trial 1 (without vacancy and hydrogen) is also shown in Table 3. The values for Trial 2 and Trial

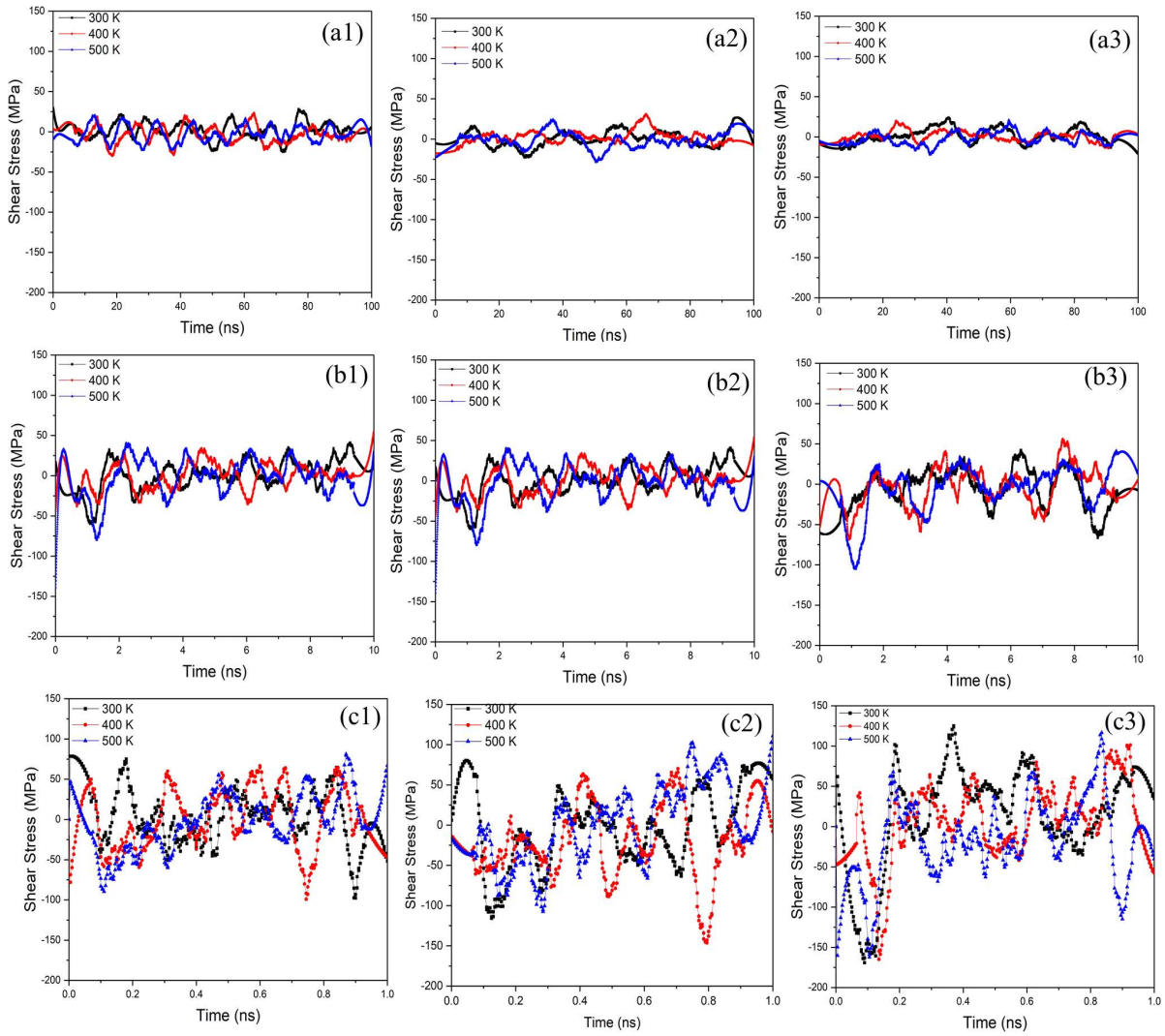

Fig. 4. Shear stress evolution with time at different temperatures for Trial 3 with 1V1 (a1, b1, and c1), 2V1 (a2, b2, and c2), and 1V2 (a3, b3, and c3): The dislocation velocity of (a1–a3), (b1–b3), and (c1–c3) are 0.1, 1, and 10 m/s, respectively. (Online version in color.)

Table 3. Average shear stress for various conditions.

Conditions		Average shear stress [MPa]								
		10 m/s			1 m/s			0.1 m/s		
		300 K	350 K	400 K	300 K	350 K	400 K	300 K	350 K	400 K
Trial 1		4.8	3.7	0.6	2.9	3.5	0.5	1.4	1.1	0.02
Trial 2	C_H=0.5 nm^{-1}	–	–	–	–	–	–	35.2	30.0	18.2
	C_H=1 nm^{-1}	–	–	–	–	–	–	47.9	36.7	24.4
	C_H=2.5 nm^{-1}	–	–	–	–	–	–	241.9	158.8	46.7
	C_H=5 nm^{-1}	–	–	–	–	–	–	347.8	166.3	120.6
Trial 3	1V1	24.8	24.1	22.3	3.8	3.1	2.7	2.0	3.2	0.9
	2V1	29.2	19.0	20.4	9.1	4.7	6.6	8.4	1.7	0.6
	1V2	32.0	33.4	27.8	14.5	7.4	4.5	3.6	2.7	2.0
Trial 4	VH1	–	–	–	–	–	–	31.4	30.5	19.9
	VH2	–	–	–	–	–	–	39.8	36.2	26.8
	VH3	–	–	–	–	–	–	75.4	68.5	57.7

4 were reported only for V_d=0.1 m/s cases because the dragging motion of hydrogen atoms by dislocation does not occur at higher dislocation speeds.

At a high-dislocation speed (≥1 m/s), the hydrogen atoms show a pinning effect, resulting in a large peak at the beginning of the shear stress curves, particularly for 10 m/s cases (Figs. 3(c1)–3(c4)). However, at low-dislocation speed (≤0.1 m/s), the hydrogen atmosphere moves with the dislocation via diffusion, and the hydrogen atoms provide continuous resistance to the movement of the dislocations because of solute drag (Figs. 3(a3) and 3(a4)). The pinning of the dislocation by the collective interaction with hydrogen atoms has been reported in other material system[40] and can be attributed to a similar phenomenon. The shear stress was greatest in the sample with the highest concentration of hydrogen. Hydrogen has a smaller influence on edge-dislocation mobilities with decreased shear stress, as temperature increases. Although the interatomic potential used in this study is different from the previous study,[24] the hydrogen effect on the mobility of edge dislocations is similar.

The vacancy effect on dislocation mobility is significantly different from the hydrogen effect. The temperature has little effect on the shear stress required to migrate the edge dislocations in the presence of vacancy and without hydrogen (Fig. 4). The results show that the necessary shear stress fluctuates, but the average value with time is very small compared with the hydrogen effect for V_d=0.1 m/s case (Table 3).

Figure 5 demonstrates the absorption of V1. When a vacancy collides with an edge dislocation, it is absorbed by the dislocation, resulting in the formation of a jog on the dislocation line (see Fig. 5(d)). Figure 5 only displayed the result at 0.1 m/s. At all dislocation velocities (including V_d>10 m/s), the same behaviors were also observed. Although the effect of vacancy concentration on the edge dislocation motion was very small in this analysis, the sample with 1V2 has a slightly greater impact on edge-dislocation mobility with greater shear stress (Table 3).

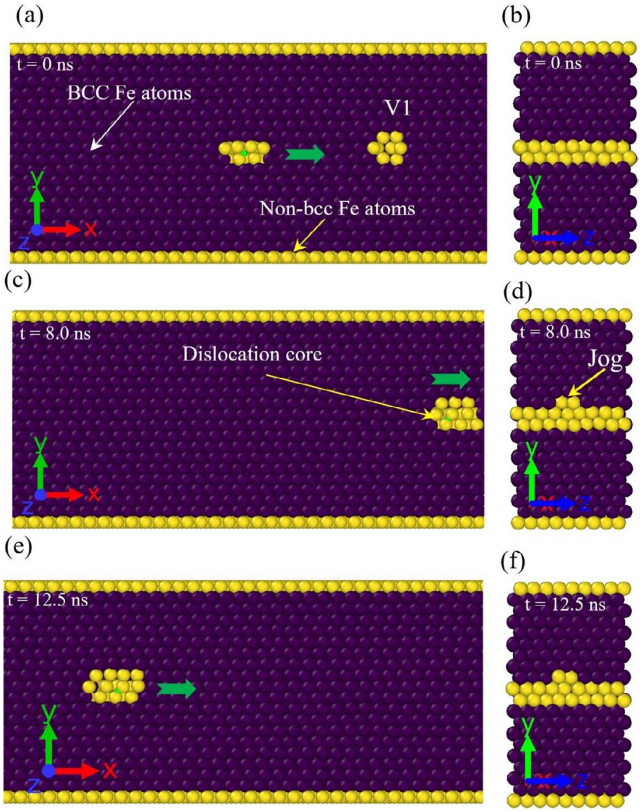

Fig. 5. Interaction of an edge dislocation with V1 at V_d = 0.1 m/s: (a) and (b) before V1 absorption at t = 0 ns. (c) and (d) After V1 is absorbed at t = 8.0 ns and jog formation. (e) and (f) jog migration with dislocation at t = 12.5 ns. (a), (c) and (e) depicts the cross-section viewed in a x-coordinate while (b), (d) and (f) depicts the cross-section viewed in an z-coordinate. (Online version in color.)

3.2. Influence of Hydrogen-vacancy Complexes on Edge Dislocation Motion

The differences in reactions of VH1 at 0.1 m/s and VH1 at 10 m/s when an edge dislocation interacts with them are shown in **Figs. 6**(a), 6(b). Only the VH1 system was shown in Figs. 6(a) and 6(b) because the three instances (*i.e.* VH1,

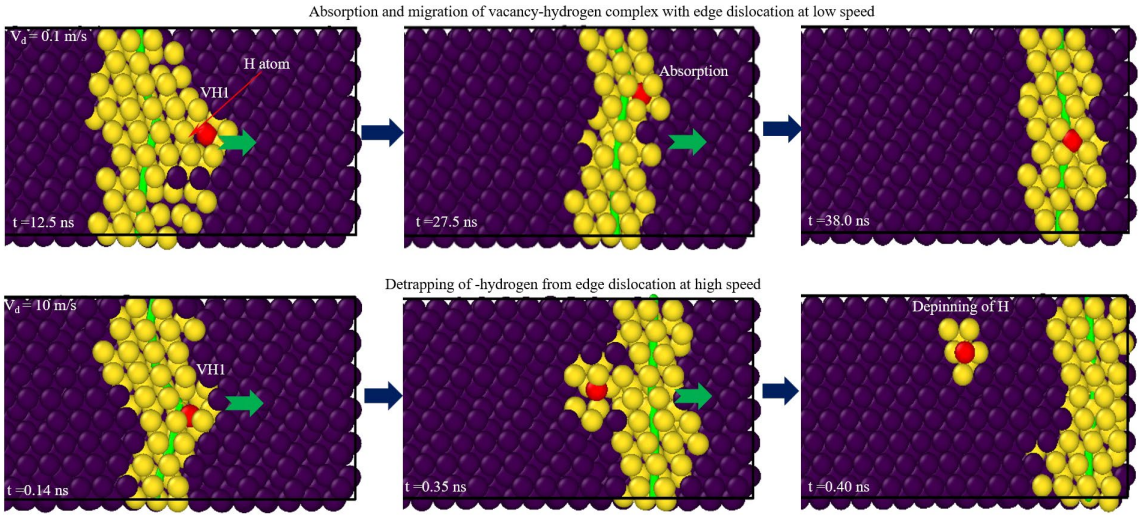

Fig. 6. Instances that demonstrate the hydrogen-vacancy complex when it interacts with edge dislocations at 300 K. The cross sections are viewed on the y-axis. (a) Interaction with VH1 at a gliding velocity ≤ 0.1 m/s (b) Interaction with VH1 at high dislocation velocity regimes ($V_d \geq 1$ m/s). (Online version in color.)

VH2, and VH3) exhibit similar behavior as shown in the figures. At a low glide dislocation velocity ($V_d \leq 0.1$ m/s), our MD simulation revealed that the dislocation absorbed the hydrogen-vacancy complex in the slip plane and caused the hydrogen and the jog (vacancy) to migrate along with the edge dislocation (Fig. 6(a)). The movement of hydrogen and vacancy with the edge dislocation segment becomes easier at low dislocation velocity regimes because hydrogen has more time to catch up with the dislocation motion.

However, the same phenomenon is not observed when an edge dislocation collides with a VH*n* complex at higher dislocation speeds ($V_d \geq 1$ m/s). VH*n* complex shows higher stability when colliding with edge dislocations during plastic deformation at higher dislocation speeds in contrast to the observation at low gliding speed. Hydrogen does not migrate with dislocation because the gliding velocity is too fast for hydrogen to catch up. When the dislocation's gliding velocity is high, the hydrogen cannot follow the dislocation motion, resulting in the formation of an isolated hydrogen detached from the dislocation and diffused into the material (Fig. 6(b)).

Figure 7 shows the VH*n* impact on the shear stress to migrate the edge dislocation. The shear stress is highest in α-iron with VH3 at all temperatures, followed by VH2 and VH1 at the lowest (Figs. 7(a3), 7(b3), and 7(c3)). The shear stress in all cases decreases as temperature increases. The average shear stress for dislocation migration in the presence of VH1, VH2, and VH3 is close to $C_H = 0.5$ nm^{-1}, $C_H = 1$ nm^{-1}, and between $C_H = 1$ nm^{-1} and $C_H = 2.5$ nm^{-1} respectively (Table 3), confirming that the hydrogen concentration along the dislocation line after absorption controls the required average shear stress for migration.

Figure 8 shows the time evolution of shear stress and edge dislocation motion at 300 K for Trial 5 with five 1VH2 arranged on the slip plane along the dislocation path and at dislocation velocity of 0.1 m/s. At first, the five VH2 were arranged in a line (Fig. 8(b1)). The dislocation gradually moves and absorbs the first two VH2 with the hydrogen atoms around the dislocation core (Fig. 8(b2)), corresponding to the first peak stress in Fig. 8(a). At ~65 ns, all the five VH2 have already been absorbed (Fig. 8(b3)). Here, the same part of the dislocation segment interacts with multiple hydrogen-vacancy complexes, resulting in a large jog. The peak value of shear stress measured here was ~450 MPa. After this point, some hydrogen-vacancy complexes are left behind, free from dislocation trapping with the sharp decrease in shear stress at ~90 ns (Fig. 8(a)); only the dislocation core with a few hydrogen-vacancy complexes move forward (Fig. 8(b4)). This result shows the dislocation pinning of hydrogen-vacancy complexes and the depinning process when the jog becomes too large at a low-speed dislocation migration.

The influence of the hydrogen-vacancy complex on dislocation mobility was also confirmed when five VH2 were arranged at different positions in the z-coordinate (**Fig. 9**(b)). Here, the dislocation absorbed all the five VH2 at different parts and migrated with the dislocation. The hydrogen-vacancy complexes act as hydrogen tanks in the crystal. They supply hydrogen atoms to the dislocation and increases the shear stress necessary to migrate the dislocation. The required shear stress increases with the number of hydrogen atoms along the dislocation. The peak shear stress is slightly greater than in the ten hydrogen case ($C_H = 5$ nm^{-1} and $V = 0.1$ m/s case of Trial 2, Fig. 3(a4)), and the value is higher than 800 MPa (Fig. 8(a)).

The concentration (atomic ratio) of hydrogen in a lattice is extremely low, typically less than ppm order, in α-iron. On the other hand, the concentration of vacancy type defects is reported to be 0.1% order after the plastic deformation under hydrogen environment.[8] As a result, there is frequent interaction between hydrogen-vacancy complexes and mobile dislocations. Our calculation showed that the hydrogen-vacancy complexes act as hydrogen tanks and supply hydrogen atoms to the edge dislocations. Hence, the edge dislocations sweep and absorb more hydrogen atoms than without hydrogen-vacancy complexes during their migration if the high-density complexes are formed. As a result, the mobility of edge dislocations is lost very quickly, and it can enhance the activity of screw dislocations to cause the same amount of deformation. The activities of

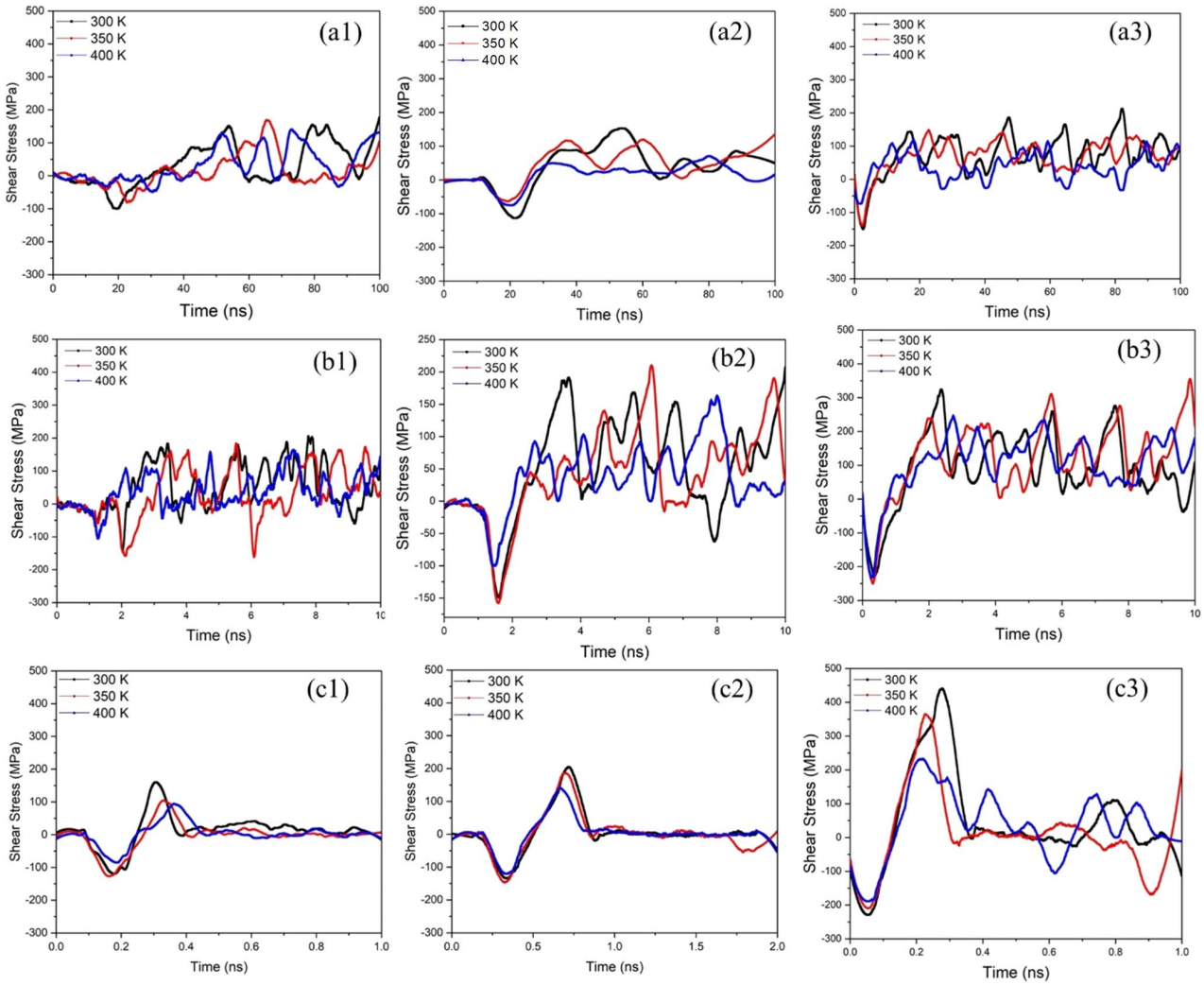

Fig. 7. Shear stress evolution with time at different temperatures for Trial 4 with VH1 (a1, b2, and c1), VH2 (a2, b2, and c2), and VH3 (a3, b3, and c3): The dislocation velocity of (a1–a3), (b1–b3), and (c1–c3) are 0.1, 1, and 10 m/s, respectively. (Online version in color.)

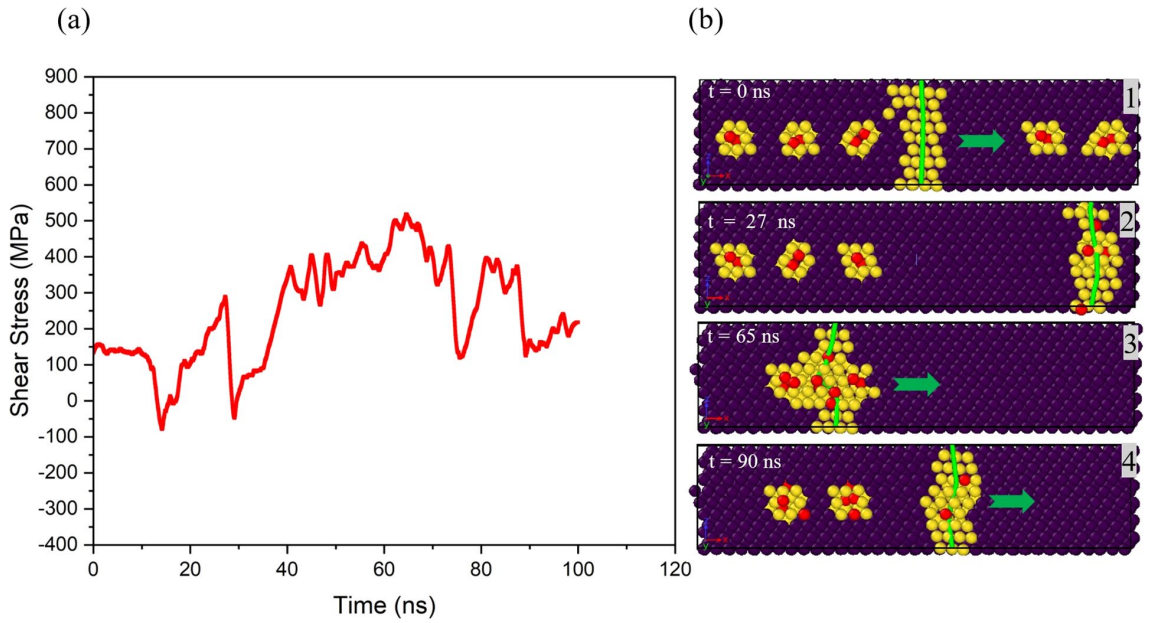

Fig. 8. (a) Time evolution of shear stress for Trial 5 with five 1VH2 and (b) the motion of edge dislocation at dislocation velocity of 0.1 m/s at 300 K: All VH2 were arranged in a line to interact with the same part of dislocation line. (Online version in color.)

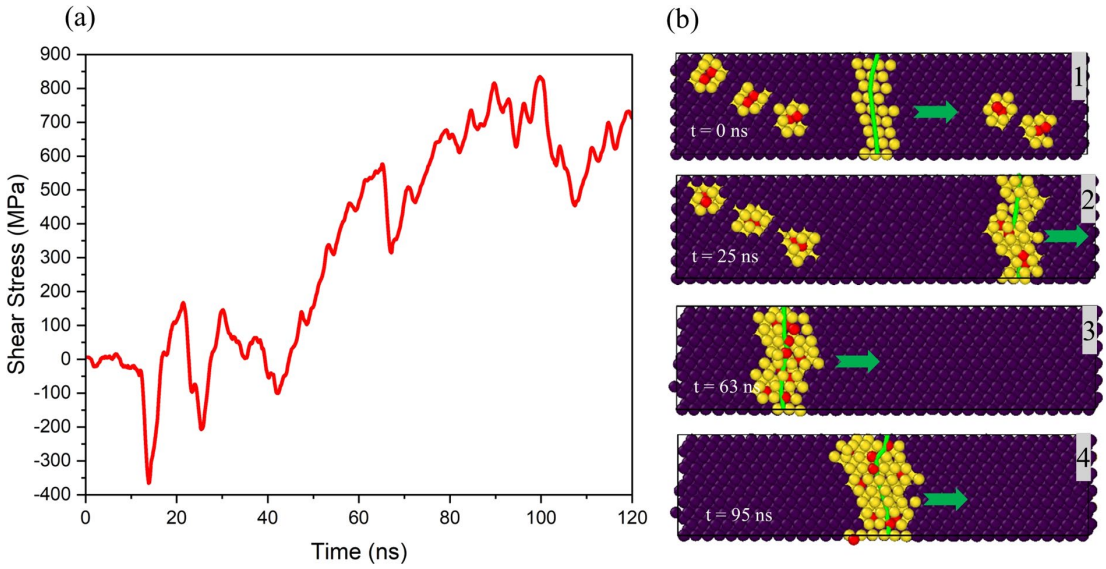

Fig. 9. (a) Time evolution of shear stress for the second Trial 5 model with five 1VH2 and (b) the motion of edge dislocation at the dislocation velocity of 0.1 m/s at 300 K: VH2 are arranged at different positions along z direction to interact with a different part of dislocation line. (Online version in color.)

screw dislocations can nucleate more vacancy-type defects and form hydrogen-vacancy complexes that prevent the next edge-dislocation migration. This cycle possibly increases the local defect density and enhances damage accumulation, reducing ductility. The screw-dislocation motion can also be influenced by hydrogen. However, the hydrogen-trap energy of screw dislocation is much smaller than edge dislocation; thus, the hydrogen concentration at screw dislocation does not increase as edge dislocation during migration. So, it is considered that hydrogen effects on screw dislocation are not added up during migration.

4. Conclusions

This study used MD simulations and the accurate embedded-atom method (EAM) force field to investigate the average shear stress required to initiate edge dislocation mobility in α-iron containing vacancy and hydrogen-vacancy complexes as a function of temperature ranging from 300 to 500 K and dislocation velocity ranging from 0.1 to 10 m/s. The results are summarized as follows.

(1) The required shear stress to glide edge dislocation in α-iron containing only vacancy is very small in all cases when averaged over time. Furthermore, at all dislocation velocities and temperatures treated in this paper, the dislocation absorbs the vacancies in the slip plane and causes them to migrate with the edge dislocation. The sample with a divacancy (1V2) has a slightly greater impact on edge-dislocation mobility with greater shear stress.

(2) At low dislocation velocity regimes ($V_d \leq 0.1$ m/s), the dislocation absorbs the hydrogen-vacancy complexes along the slip plane and causes them to migrate with the edge dislocation. Thus, the drag effect of the hydrogen-vacancy complex is continuous. At higher dislocation speeds ($V_d \geq 1$ m/s), hydrogen does not migrate with the dislocation, resulting in the formation of isolated hydrogen detached from the dislocation and diffused into the material; only vacancy is absorbed. After all, the hydrogen-vacancy complexes significantly impact edge-dislocation mobilities with increasing shear stress at a lower temperature and a larger number of hydrogen in vacancy.

(3) When the edge dislocation interacts with multiple hydrogen-vacancy complexes at a lower dislocation velocity ($V_d = 0.1$ m/s), the dislocation absorbs the complexes if they interact with dislocation at different points rather than at a single point to avoid the formation of a large jog at the colliding segment. The hydrogen-vacancy complexes act as hydrogen tanks in the crystal. They supply the hydrogen atoms to the dislocation, increase the shear stress, and cause the dislocation to migrate almost linearly as it travels.

Acknowledgement

This research was supported by ISIJ Research Promotion Grant and JSPS KAKENHI Grant Number 19H02025.

REFERENCES

1) M. Nagumo: Fundamentals of Hydrogen Embrittlement, Springer Singapore, (2016). https://doi.org/10.1007/978-981-10-0161-1
2) J. P. Hirth: *Metall. Trans. A*, **11** (1980), 861. https://doi.org/10.1007/BF02654700
3) J. B. Condon and T. Schober: *J. Nucl. Mater.*, **207** (1993), 1. https://doi.org/10.1016/0022-3115(93)90244-S
4) R. Matsumoto, S. Seki, S. Taketomi and N. Miyazaki: *Comput. Mater. Sci.*, **92** (2014), 362. https://doi.org/10.1016/j.commatsci.2014.05.029
5) M. Nagumo and K. Takai: *Acta Mater.*, **165** (2019), 722. https://doi.org/10.1016/j.actamat.2018.12.013
6) Y. Sugiyama and K. Takai: *Acta Mater.*, **208** (2021), 116663. https://doi.org/10.1016/j.actamat.2021.116663
7) P. Gong, I. H. Katzarov, J. Nutter, A. T. Paxton and W. M. Rainforth: *Sci. Rep.*, **10** (2020), 1. https://doi.org/10.1038/s41598-020-66965-z
8) S. Li, Y. Li, Y. C. Lo, T. Neeraj, R. Srinivasan, X. Ding, J. Sun, L. Qi, P. Gumbsch and J. Li: *Int. J. Plast.*, **74** (2015), 175. https://doi.org/10.1016/j.ijplas.2015.05.017
9) L. Chiari and M. Fujinami: *ISIJ Int.*, **62** (2022), 832. https://doi.org/10.2355/isijinternational.isijint-2021-422
10) P. J. Ferreira, I. M. Robertson and H. K. Birnbaum: *Acta Mater.*, **46** (1998), 1749. https://doi.org/10.1016/S1359-6454(97)00349-2
11) A. H. M. Krom and A. D. Bakker: *Metall. Mater. Trans. B*, **31** (2000), 1475. https://doi.org/10.1007/s11663-000-0032-0
12) P. R. Monasterio, T. T. Lau, S. Yip and K. J. Van Vliet: *Phys. Rev. Lett.*, **103** (2009). https://doi.org/10.1103/PhysRevLett.103.085501
13) S. Taketomi and R. Matsumoto: Atomistic Simulations of Hydrogen Effects on Lattice Defects in Alpha Iron, in: Handb. Mech. Mater.,

Springer Singapore, (2019), 283. https://doi.org/10.1007/978-981-10-6884-3_11
14) J. Song and W. A. Curtin: *Acta Mater.*, **68** (2014), 61. https://doi.org/10.1016/j.actamat.2014.01.008
15) A. Barnoush, M. Asgari and R. Johnsen: *Scr. Mater.*, **66** (2012), 414. https://doi.org/10.1016/j.scriptamat.2011.12.004
16) H. Yu, A. Cocks and E. Tarleton: *J. Mech. Phys. Solids.*, **123** (2019), 41. https://doi.org/10.1016/j.jmps.2018.08.020
17) I. H. Katzarov, D. L. Pashov and A. T. Paxton: *Phys. Rev. Mater.*, **1** (2017), 1. https://doi.org/10.1103/PhysRevMaterials.1.033602
18) E. Hayward and C. Deo: *J. Phys. Condens. Matter.*, **23** (2011). https://doi.org/10.1088/0953-8984/23/42/425402
19) G. Lu and E. Kaxiras: *Phys. Rev. Lett.*, **94** (2005), 1. https://doi.org/10.1103/PhysRevLett.94.155501
20) Y. Tateyama and T. Ohno: *Phys. Rev. B - Condens. Matter Mater. Phys.*, **67** (2003), 1. https://doi.org/10.1103/PhysRevB.67.174105
21) E. Hayward and C. C. Fu: *Phys. Rev. B - Condens. Matter Mater. Phys.*, **87** (2013), 1. https://doi.org/10.1103/PhysRevB.87.174103
22) R. Matsumoto, N. Nishiguchi, S. Taketomi and N. Miyazaki: *J. Soc. Mater. Sci. Japan.*, **63** (2014), 182. https://doi.org/10.2472/jsms.63.182
23) K. Ohsawa, K. Eguchi, H. Watanabe, M. Yamaguchi and M. Yagi: *Phys. Rev. B - Condens. Matter Mater. Phys.*, **85** (2012), 1. https://doi.org/10.1103/PhysRevB.85.094102
24) R. Matsumoto, S. Oyinbo, M. Vijendran and S. Taketomi: *ISIJ Int.*, (2022). https://doi.org/10.2355/isijinternational.isijint-2022-311
25) S. Taketomi, R. Matsumoto and N. Miyazaki: *Acta Mater.*, **56** (2008), 3761. https://doi.org/10.1016/j.actamat.2008.04.011
26) S. Taketomi, R. Matsumoto and N. Miyazaki: *J. Mater. Res.*, **26** (2011), 1269. https://doi.org/10.1557/jmr.2011.106
27) S. Taketomi, R. Matsumoto and S. Hagihara: *ISIJ Int.*, **57** (2017), 2058. https://doi.org/10.2355/isijinternational.ISIJINT-2017-172
28) S. Plimpton: *J. Comput. Phys.*, **117** (1995), 1. https://doi.org/10.1039/c7sm02429k
29) A. Stukowski: *Model. Simul. Mater. Sci. Eng.*, **18** (2010). https://doi.org/10.1088/0965-0393/18/1/015012
30) H. J. C. Berendsen, J. P. M. Postma, W. F. Van Gunsteren, A. Dinola and J. R. Haak: *J. Chem. Phys.*, **81** (1984), 3684. https://doi.org/10.1063/1.448118
31) A. Stukowski and K. Albe: *Model. Simul. Mater. Sci. Eng.*, **18** (2010). https://doi.org/10.1088/0965-0393/18/8/085001
32) J. D. Honeycutt and H. C. Andemen: *J. Phys. Chem.*, **1** (1987), 4950. https://doi.org/10.1021/j100303a014
33) D. Cereceda, A. Stukowski, M. R. Gilbert, S. Queyreau, L. Ventelon, M. C. Marinica, J. M. Perlado and J. Marian: *J. Phys. Condens. Matter.*, **25** (2013). https://doi.org/10.1088/0953-8984/25/8/085702
34) M. R. Gilbert, S. Queyreau and J. Marian: *Phys. Rev. B - Condens. Matter Mater. Phys.*, **84** (2011), 1. https://doi.org/10.1103/PhysRevB.84.174103
35) J. Sanchez, J. Fullea, M. C. Andrade and P. L. De Andres: *Phys. Rev. B - Condens. Matter Mater. Phys.*, **81** (2010), 8. https://doi.org/10.1103/PhysRevB.81.132102
36) N. H. Nguyen, R. Henning and J. Z. Wen: *J. Nanoparticle Res.*, **13** (2011), 803. https://doi.org/10.1007/s11051-010-0082-4
37) M. Wen: *Comput. Mater. Sci.*, **197** (2021), 110640. https://doi.org/10.1016/j.commatsci.2021.110640
38) J. Song, W. A. Curtin: *Nat. Mater.*, **12** (2013), 145. https://doi.org/10.1038/nmat3479
39) Y. Cui, C. Hu, P. Yu, D. Xie, L. Kong, Y. Rong, M. Wen and J. Zou: *Mater. Res. Express.*, **7** (2020), 1. https://doi.org/10.1088/2053-1591/ab9a81
40) D. Xie, S. Li, M. Li, Z. Wang, P. Gumbsch, J. Sun, E. Ma, J. Li and Z. Shan: *Nat. Commun.*, **7** (2016). https://doi.org/10.1038/NCOMMS13341